Nanoscale

COMMUNICATION

View Article Online
View Journal | View Issue

Cite this: *Nanoscale*, 2019, **11**, 15794

Received 16th April 2019,
Accepted 29th July 2019

DOI: 10.1039/c9nr03264a

rsc.li/nanoscale

Outer–inner dual reinforced micro/nano hierarchical scaffolds for promoting osteogenesis†

Jincheng Tang,‡[a] Yong Gu,‡[a] Hongbo Zhang,‡[b,c] Liang Wu,‡[a] Yun Xu,[a] Jiannan Mao,[a] Tianwen Xin,[a] Tingjun Ye,[b] Lianfu Deng,[b] Wenguo Cui,*[b] Hélder A. Santos*[d,e] and Liang Chen*[a]

Biomimetic scaffolds have been extensively studied for guiding osteogenesis through structural cues. Inspired by the natural bone growth process, we have employed a hierarchical outer–inner dual reinforcing strategy, which relies on the interfacial ionic bond interaction between amine/calcium and carboxyl groups, to build a nanofiber/particle dual strengthened hierarchical silk fibroin scaffold. This scaffold can provide an applicable form of osteogenic structural cue and mimic the natural bone forming process. Owing to the active interaction between compositions located in the outer pore space and the inner pore wall, the scaffold has over 4 times improvement in the mechanical properties, followed by a significant alteration of the cell–scaffold interaction pattern, demonstrated by over 2 times elevation in the spreading area and enhanced osteogenic activity potentially involving the activities of integrin, vinculin and Yes-associated protein (YAP). The *in vivo* performance of the scaffold identified the inherent osteogenic effect of the structural cue, which promotes rapid and uniform regeneration. Overall, the hierarchical scaffold is promising in promoting uniform bone regeneration through its specific structural cue endowed by its micro–nano construction.

Introduction

As the eternal subject of tissue engineering concerning orthopedic clinical practice, regeneration of bone has been studied comprehensively through diverse strategies and methodologies. Currently, concerning the construction of bone regenerative scaffolds, most efforts have been based on two basic elements: the constituent elements and the structural factor of the scaffold. The composition of the bio-scaffold can be very diverse varying from bioactive factors,[1,2] osteoconductive ingredients[3,4] to stem cells with regenerative capacity.[5] Various combinations of these constituents have been studied and extraordinary regenerative effectiveness can indeed be identified with the help of incorporation strategies.[6,7] Yet, due to the application of the exogenous bioactive elements, there are also critical problems that remain unsolved, such as uncontrolled regeneration and potential cancer risk that hindered further clinical applications of these scaffolds.[8,9] Biomimetic scaffolds ranging from traditional porous scaffolds[10,11] to emerging nanofibrous structures[12,13] have been applied to mimic the natural structure of human bone. However, only a limited amount of works have been conducted in this field and the structural cues from the sophisticated structure during the natural repairing process together with its underlying mechanism are yet to be explored.

Constructed with a fibrous collagen phase along with hydroxyapatite stacked within the fiber following an intricate order, natural bone exhibits extraordinary mechanical stability and superior regenerative capacity.[14] In the context of bone regeneration after injury, natural bone formation starts with the infiltration of granulation tissue and the formation of callus that provides the temporary fixation effect and the nutrition and calcium needed in the following step.[15] Then, stem cell activation is responsible for deposition of the extracellular matrix at the defect site, playing a key role in the regeneration process. In this process, an abundant nanofibrous matrix network serves as the template for cell–matrix interaction and hydroxyapatite deposition.[16] Finally, further mineralization

[a]*Department of Orthopedics, the First Affiliated Hospital of Soochow University, Orthopedic Institute, Soochow University, 708 Renmin Road, Suzhou, Jiangsu 215006, P.R. China. E-mail: chenliang1972@sina.com*
[b]*Shanghai Key Laboratory for Prevention and Treatment of Bone and Joint Diseases, Shanghai Institute of Traumatology and Orthopaedics, Ruijin Hospital, Shanghai Jiao Tong University School of Medicine, 197 Ruijin 2nd Road, Shanghai 200025, P.R. China. E-mail: wgcui80@hotmail.com*
[c]*Department of Pharmaceutical Sciences Laboratory and Turku Center for Biotechnology, Åbo Akademi University, Turku, 20520, Finland*
[d]*Drug Research Program, Division of Pharmaceutical Chemistry and Technology, Faculty of Pharmacy, University of Helsinki, Helsinki FI-00014, Finland*
[e]*Helsinki Institute of Life Science (HiLIFE), University of Helsinki, Helsinki FI-00014, Finland. E-mail: helder.santos@helsinki.fi*

†Electronic supplementary information (ESI) available. See DOI: 10.1039/c9nr03264a

‡These authors contributed equally to this work.

and remodeling of this nanofibrous network contribute to the regeneration and it is also synchronized with the degradation of the supporting tissue. Compared with the artificial scaffold, the natural repairing complex consists of a micron-scale supporting tissue and a nanofibrous matrix network, which can potentially affect the cellular activity and promote the inside-out repairing process through their specific structural elements.[17] Enlightened by such a natural process, we hypothesize that the highly biomimetic scaffold can be further tailored to simulate the natural repairing process of human bone in order to promote the regeneration in a more natural-like manner.

As the most abundant protein in the organic phase of natural bone, collagen has been widely reported in the biomimetic reconstruction of bone due to its predominant biological performance. However, current applicable forms of collagen to reproduce the natural extracellular matrix network, such as electrospun scaffolds and self-assembled hydrogels,[18,19] have been generally limited due to insufficient mechanical properties and stability. In addition, the silk fibroin (SF) porous scaffold, as another traditional form of bone tissue engineering scaffold, has generally failed to provide a microenvironment as an extracellular matrix. Moreover, the addition of an inorganic phase, such as hydroxyapatite (HA) or bioactive glass (BG) has been reported to bring superior osteoconductivity and mechanical properties, potentially involving ionic bonds between calcium in the inorganic ingredient and abundant carboxyl/hydroxyl groups in silk fibroin.[20] Owing to the frequent presence of amine groups in the molecular chain, collagen has been reported to act as a positively charged composition for layer-by-layer (LBL) technology, while silk fibroin, due to the abundant carboxyl and hydroxyl groups, tends to interact with both amine-rich collagen[21] and calcium containing bioglass particles[22] through ionic bonds. Therefore, such an interaction between silk fibroin scaffolds and nano-collagen/bioglass nanoparticles that, respectively, existed in the pore space and inside the backbone, could become a potential solution to break through the limitation of simple physical stacking and construct a hierarchical structure with better integrity and a higher resemblance to the complex for natural bone repairing.

Inspired by natural bone construction, a hierarchical inner–outer dual reinforcing strategy is employed to build a biomimetic hierarchical micro–nano scaffold (Scheme 1A). It is produced by integrating amine-rich nanofibrous collagen and calcium-containing bioglass nanoparticles into both the outer and inner spaces of the carboxyl-rich silk fibroin microporous backbone through active interfacial ionic bonds. The scaffold has a stable hierarchical structure along with superior mechanical properties and its capability to promote adhesion and spreading of cells. Unlike the existing microporous scaffold which generally relies on the incorporation of bioactive factors or progenitor cells, the current scaffold could promote osteogenic differentiation of autologous stem cells, and guide the structure-induced reconstruction of the damaged bone without the help of exogenous factors or cells (Scheme 1).

In this study, the physicochemical properties of the scaffolds were fully characterized to highlight the benefit of micro–nano integration in improving the bulk properties of

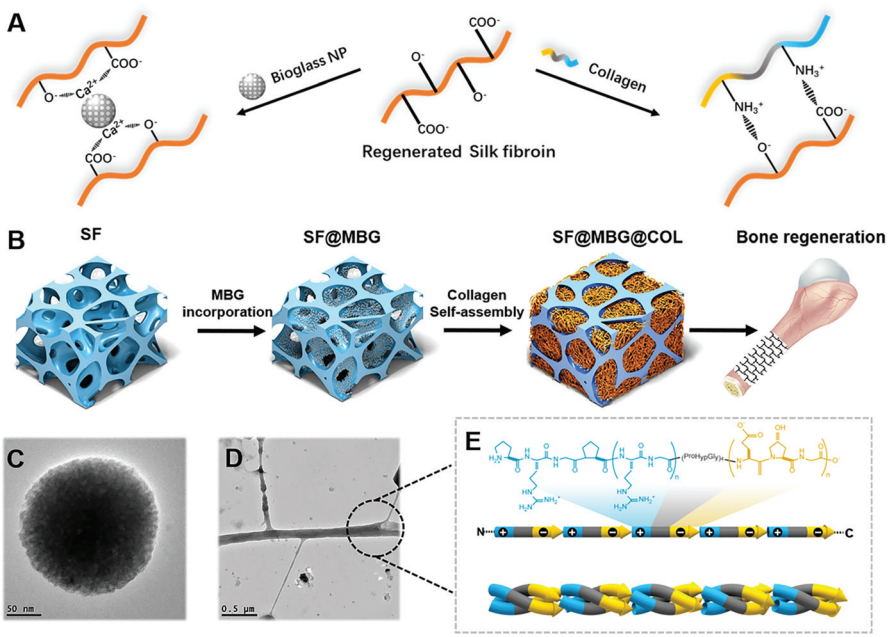

Scheme 1 Schematic illustration of (A) the ionic interaction between silk fibroin and collagen/bioglass. (B) The building process of the hierarchical scaffold for structural regeneration of bone. The representative TEM image of (C) bioglass mesoporous nanoparticles and (D) collagen assembled fiber with (E) the illustration of the assembly mechanism.

the scaffold. The biological response of bone marrow mesenchymal stem cells (BMSCs) co-cultured with scaffolds was also investigated to demonstrate the potential involved mechanism, achieving a first look into the specific osteogenic pathways of the three-dimensional micro–nano hierarchical structure. The critical size bone defect model on Sprague Dawley (SD) rats was employed to study the regenerative patterns of the bioscaffold with radiological and histological methods, which investigated the reconstruction details of bone defects.

Results and discussion

Compared with the prevailing strategy involving osteo-inductive factors and bone progenitor cells, promoting bone formation through a biomimetic structure represents a comparatively gentler way to restore the damaged tissue. Despite its inferior bioactivity, the capability to guide the osteogenic activity of progenitor cells was impregnated within the physical and biochemical cues of the hierarchical micro–nano structure,[23] which could contribute to the osteogenic effect that further imitates the natural healing process after damage of the bone tissue.

In this study, the hierarchical scaffold was prepared stage by stage as illustrated in Scheme 1B with SF indicating the bare SF scaffold, SF@MBG indicating the MBG-incorporated micro-porous SF scaffold and SF@MBG@Col indicating the collagen self-assembled micro–nano hierarchical scaffold. Both the hierarchical and non-hierarchical scaffolds were characterized for their morphology, composition and mechanical properties.

Construction and integration of the applicable form of the micro–nano biomimetic structure in the scaffold was the first step in our attempt. The silk fibroin scaffold with interconnected micro-scale pores was internally reinforced with calcium-containing mesoporous bioactive glass (MBG) nanoparticles[24] to act as a temporal skeleton, while the nanofibrous collagen matrix (Col) was self-assembled *in situ* within the pores[25] to accomplish the inner–outer dual reinforcing building of the biomimetic micro–nano structure (Scheme 1). Firstly, the successful crosslinking within the microporous scaffold structure was identified *via* Fourier transform infrared spectroscopy (FTIR) (Fig. S1A†), which indicated enhanced formation of β-sheets with an increasing amount of glycerol. Subsequently, mesoporous bioglass nanoparticles were synthesized and found to possess uniform particle size as detected by scanning electron microscopy (SEM), transmission electron microscopy (TEM) and dynamic light scattering (DLS) (Fig. S1B and C†).

The surface morphology of the constructed scaffolds was monitored by SEM. Micron-scale interconnected pores were seen in all groups (Fig. 1A). Incorporation of mesoporous bioglass (MBG) in the scaffold was identified through the appearance of white particles on the surface of the pore wall in

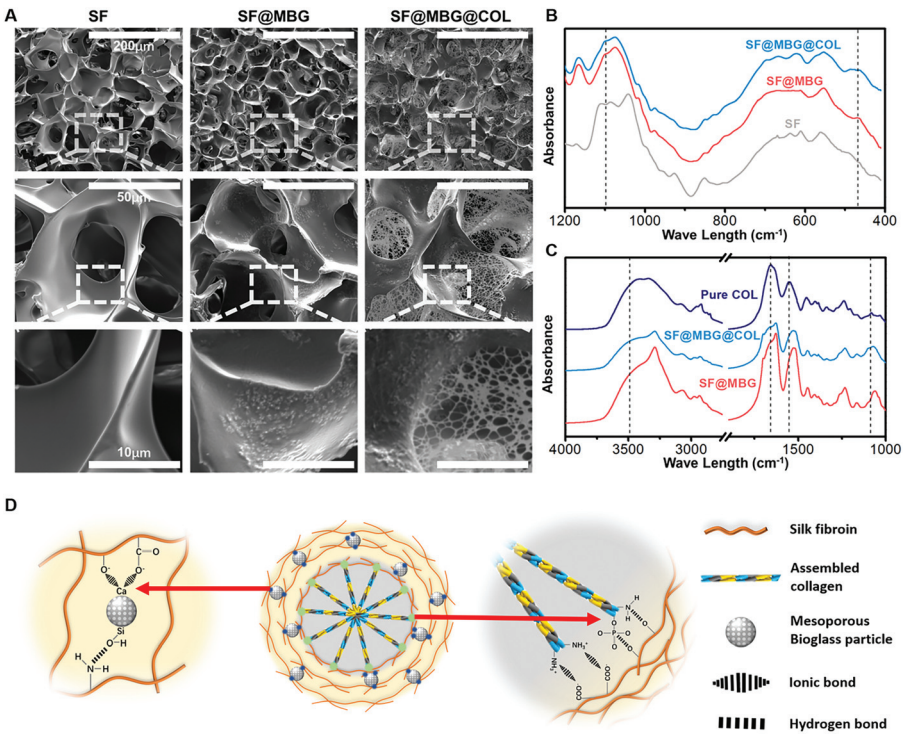

Fig. 1 Characterization of the morphology and composition. (A) SEM images of various scaffolds. (B) FTIR spectra indicating the incorporation of MBG. (C) FTIR spectra indicating the integration of Col I with pure collagen as the control. (D) The schematic illustration of the hierarchical outer–inner dual reinforcing strategy.

scaffolds containing MBG (SF@MBG), as compared with the bare silk fibroin scaffold control (SF). A slight and insignificant ($p > 0.05$) decrease in the pore sizes was detected after the incorporation of MBG (72.2 ± 5.5 μm) when compared with the SF scaffold (75.8 ± 6.3 μm). When collagen was added, the nanofibrous network was captured to fill the pores of the micro-scaffold and form an observable connection with the pore wall in the scaffold dual reinforced with MBG and collagen (SF@MBG@Col), as shown in Fig. 1A. In addition to SEM, Fourier transform infrared spectroscopy (FTIR) was employed to confirm the incorporation and integration of bioglass and collagen. As shown in Fig. 1B, bands at 468 cm^{-1} and 1095 cm^{-1} were identified corresponding to the presence of bioglass. As for the verification of collagen integration, the hierarchical scaffold with self-assembled collagen was washed three times with deionized water before drying and FTIR characterization. Using pure rat tail collagen as the control, bands at around 3500 cm^{-1}, 1500–1700 cm^{-1} and 1100 cm^{-1} were found (Fig. 1C), which indicate the existence of collagen in hierarchical scaffolds and the stable integration of the collagen nanofiber within pores.

The formation of a well-integrated structure in this hierarchical scaffold significantly relied on the ionic interaction between nano-collagen/bioglass and silk fibroin. As depicted in Fig. 1D, collagen has a large amount of amine groups in its molecular chain, which are capable of forming ionic bonds with the carboxyl groups present in silk fibroin. Additionally, the bioglass was also firmly integrated to the scaffold owing to the ionic bond between the calcium content in bioglass and carboxyl groups in silk fibroin. Hence, both ingredients were found to fit well in the hierarchical structure through active ionic interaction with silk fibroin. Apart from ionic bonds, hydrogen bonds were also involved due to the abundant hydroxyl groups in silk fibroin to strengthen the integration.

Such stable integration provided the basis for further improvement of the various properties of the scaffold, among which the mechanical properties exhibited the most significant elevation that was believed to affect the fate of stem cells. Before characterization of the integrated scaffolds, the self-assembly of bare collagen was characterized by TEM and a rheology test. The nano-scale fibrous network was clearly observed in assembled collagen under a TEM (Fig. 2A), with a fiber diameter of less than 200 nm, which distributed like a spider web. Moreover, a larger G' (storage modulus) compared with G'' (loss modulus) was detected in both the strain (Fig. 2Ba) and frequency dependent rheology test (Fig. 2Bb), further indicating the successful assembly of collagen. Then, measurements of both the macro-mechanical properties and rheological performance were performed on a constructed scaffold, so as to study the effect of incorporating bioglass and the nanofibrous collagen on the scaffold mechanical properties. When comparing SF and SF@MBG, addition of bioglass nanoparticles was found to elevate the compressive modulus of the scaffold by 35% (17.0 ± 2.0 *vs.* 23.5 ± 1.0 kPa) (Fig. 2C), due to the physical incorporation and ionic integration into silk fibroin. Surprisingly, a further 3 times

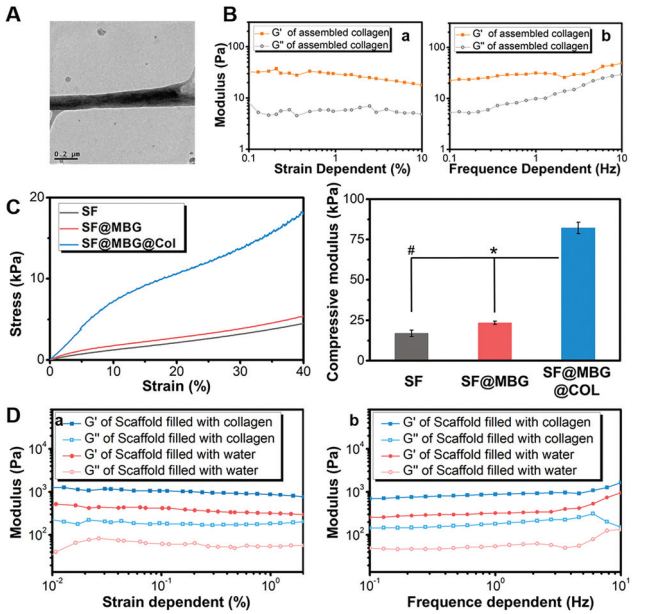

Fig. 2 Characterization of the mechanical properties and pro-mineralization capacity. (A) TEM image of the assembled collagen nanofiber. (B) Rheological behavior of assembled collagen dependent on (a) strain and (b) frequency. (C) Stress–strain curve of scaffolds and respective moduli under the uniaxial compression test. (Statistical differences are indicated with $*p < 0.05$ when comparing SF@MBG@Col and SF@MBG, $\#p < 0.05$ when comparing SF@MBG@Col and SF, and $\&p < 0.05$ when comparing SF@MBG and SF.) (D) Rheological behavior of the micro/nano scaffold *vs.* the micro scaffold in both (a) strain- and (b) frequency-dependent modes.

elevation ($p < 0.01$) of modulus (23.5 ± 1.0 *vs.* 82.2 ± 3.5 kPa) was witnessed after the integration of collagen as identified in the MBG/collagen dual reinforced scaffold (SF@MBG@Col). Generally, more than 4 times elevation (17.0 ± 2.0 *vs.* 82.2 ± 3.5 kPa) could be obtained when comparing SF@MBG@Col and SF, which relied on the collaborative effect from MBG incorporation and nano-collagen integration. Such a phenomenon was further verified by a rheological test. As shown in Fig. 2D, the storage modulus was significantly higher in the SF@MBG@Col group compared with the SF@MBG group in both the strain (Fig. 2Da) and frequency-dependent mode (Fig. 2Db), indicating the superior structural integrity of the hierarchical scaffolds. The significant improvement in the mechanical properties when comparing SF@MBG and SF@MBG@Col was thought to be related to the ionic interaction between the collagen phase and the microporous scaffold. Since all mechanical tests were conducted under wet conditions, the integration of collagen and the scaffold could be highlighted when compared with water within the SF and SF@MBG scaffolds, which flowed away under the deformation of the scaffold. Usually, the application of bare self-assembled collagen and other peptides was limited by insufficient mechanical properties in the field of tissue engineering,[26] and the glycerol-crosslinked SF scaffold was also thought to be unsuitable for bone tissue engineering due to insufficient modulus and bioactivity.[27] Herein, the inner–outer dual strengthening strat-

egy produced satisfactory mechanical properties (over 4 times elevation) with a proper modulus (82 kPa) suitable for guiding the osteogenic pathway of progenitor cells. The current scaffold is still incompetent in replicating the physical cue of natural cancellous bone that possesses a Young's modulus on the gigabit level. The biomimetic reinforcing strategy we have employed here has overcome the limitation of mechanical properties from both self-assembled collagen (under 10 kPa) and the silk fibroin microporous scaffold (under 20 kPa). Since a higher modulus of the substrate (higher than 34 kPa) was reported to contribute to the osteogenesis,[28] the improvement in the modulus here satisfied the need for guiding the stem cells to the bone lineage. Such a remarkable mechanical improvement was thought to be not only related to the physical stacking of multiple compositions, but also associated with the active interaction between silk fibroin, bioglass and collagen located in both the internal backbone and outer pore space. Furthermore, compared with the traditional two-dimensional ionic interaction applied in LBL technology,[21] the dual reinforcing strategy was applied here to build a three-dimensional scaffold, which possessed a more hierarchical organization and higher specific surface area and was capable of achieving better performance in improving the structural integrity. Improvements in the bulk properties of the scaffold not only optimized the operability and stability of the scaffold compared with the traditional electrospun or bare self-assembled scaffolds, but also provided a suitable physical environment for the induction of further differentiation. While a hierarchical organization can address the insufficiency of bulk properties, the nano-scale structure in the hierarchical structure tended to affect the adhesion, spreading and later proliferation of progenitor cells.[29] Besides the improvement in the proliferation rate, the most intuitive distinction was seen on the spreading pattern and cytoskeleton organization of cells seeded on the micro–nano scaffold, where a more stretched cytoskeleton of bone mesenchymal stem cells (BMSCs) was observed. The coordination of the micron structure and nanofibrous network can have an impact on the cell–material interaction pattern, potentially involving the activity of integrin,[30,31] vinculin[32] and Yes-associated protein (YAP),[33] all of which have been reported to regulate the cell–matrix interaction mediated by mechanical or structural cues presented by the substrate. A potential downstream osteogenic effect was observed after enhancing the vinculin and YAP activity of progenitor cells through the structural cues of substrates;[34,35] thus, we hypothesized that it is reasonable to exert the osteogenic potential *via* the bare hierarchical scaffold through the structural cues, instead of introducing bioactive factors or implanted progenitor cells.

Scaffolds with or without a hierarchical structure were seeded with BMSCs to access their bioactivity in promoting cell adhesion and proliferation. Cell adhesion and spreading was observed with the help of SEM. As demonstrated in Fig. 3A, BMSCs adhered to scaffolds from all three groups,

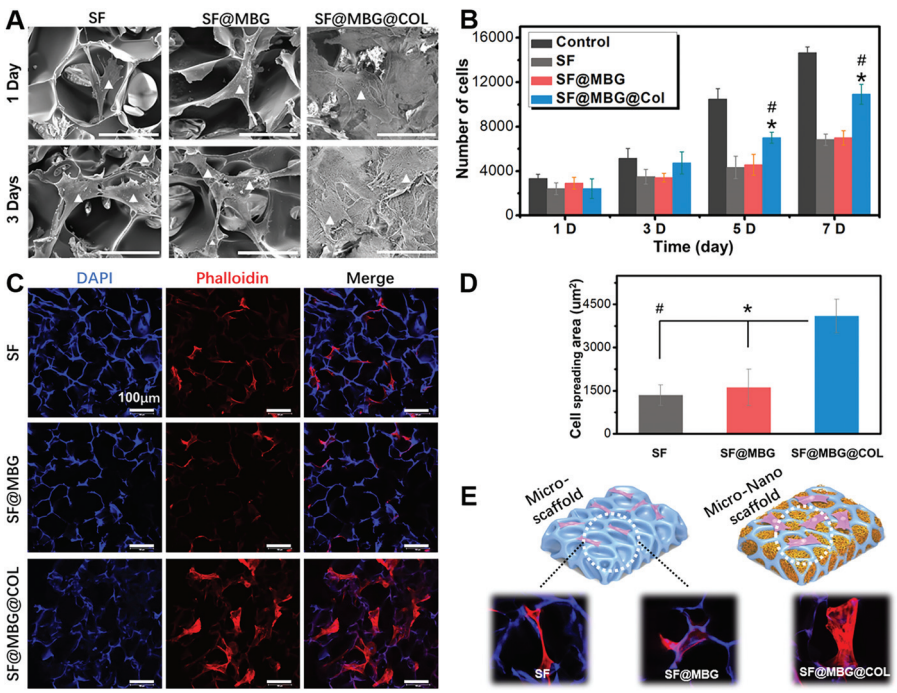

Fig. 3 Cell adhesion and proliferation assays. (A) SEM images of BMSCs (indicated by a white triangle) adhered on scaffolds. (B) Proliferation rates of BMSCs after co-culture on scaffolds for 1, 3, 5, and 7 days. (C) Phalloidin (red) and DAPI (blue) staining of BMSCs co-cultured with scaffolds for 3 days. (D) Quantification of the cell spreading area on different scaffolds. (E) Illustration of the adhesion pattern of BMSCs on scaffolds with representative fluorescent images. (Statistical differences are indicated with $*p < 0.05$ when comparing SF@MBG@Col and SF@MBG and $\#p < 0.05$ when comparing SF@MBG@Col and SF).

while the spreading conditions on SF and SF@MBG scaffolds showed no significant difference. Limited contact between cells and the scaffold was found in those two groups as indicated by the poorly stretched morphology on the pore wall. However, the hierarchical collagen network was found to bring a significantly better condition for BMSC spreading. Such differences in cellular spreading also brought improved biocompatibility, which was reflected in the proliferation rate. As indicated in Fig. 3B, despite all scaffold groups being inferior to the blank group, from day 3, a higher cell proliferation rate was found in SF@MBG@Col groups compared with SF and SF@MBG groups. It is reasonable to believe that, although all scaffolds failed to provide a proliferating platform as good as a Petri dish, scaffolds with a hierarchical structure still exhibited superior biocompatibility and bioactivity over traditional micron porous scaffolds.

The osteogenic bioactivity of the hierarchical structure was also characterized with the assessment of ALP activity and Alizarin red staining after co-culturing BMSCs with various scaffolds. By immersing the scaffolds in osteogenic medium for different periods of time (7 days and 14 days), a significantly higher ALP activity ($p < 0.05$) was detected in SF@MBG and SF@MBG@Col groups compared to the SP group (Fig. S2A and B†), while no significant difference was detected between SF@MBG and SF@MBG@Col ($p > 0.05$). As another important factor that reflects the osteogenesis activity of co-cultured BMSCs, Ca-content deposition in cells was quantified with Alizarin red staining. Denser calcium nodules were found in BMSCs co-cultured with SF@MBG and SF@MBG@Col groups on both days 14 and 21, indicating a higher osteogenic activity (Fig. S2C and D†), while no significant difference was identified between the two groups.

In order to further look into the cytoskeleton organization of co-cultured cells, actin fibers were stained with phalloidin. A totally different cellular morphology was found on SF@MBG@Col (Fig. 3C). According to the corresponding quantification, nearly 3 times elevation (4094 ± 587 *vs.* 1347 ± 360/1616 ± 628 μm^2) on the spreading area was found in SF@MBG@Col as compared with SF or SF@MBG groups ($p < 0.01$) (Fig. 3D). It is worth noting that there were also significant differences in the adhesion pattern between the hierarchical and non-hierarchical scaffolds. In SF or SF@MBG, the cells tended to adhere on the pore wall of the micron-scale scaffold, while in the SF@MBG@Col group, the hierarchical structure relieved the cells from such spatial restriction, allowing them to spread within the pore space to obtain the fully-spread state, as shown in Fig. 3E.

The coordination of the micron structure and nanofibrous network could have an important impact on the cell–material interaction and the osteogenic activity. In order to explore the underlying mechanism, we investigated several potential anticipators involved in the pro-osteogenic pathway through immunofluorescence staining and western blot, so as to seek for a clearer mechanism on how the hierarchical structure guides the fate of stem cells.

The hierarchical structure consisted of a microporous backbone and a nano-scale fibrous network was found to possess superior mechanical properties in the macroscopic view, and it is necessary to study the cell–matrix interaction on a deeper level. As indicated by the immunofluorescence staining and western blot results, a higher expression of integrin was detected within stem cells seeded on the micro–nano hierarchical structure. As the major regulator in the cell–matrix interaction, integrin bridges the gap between the endocellular signal pathway and the extracellular matrix protein.[30,31] Interactions between the stem cells and biomimetic scaffold that were thought to begin with the activation of integrin, resulted from the recognition and binding of the receptor and cellular-adhesive peptide.[36] The activity of β-integrin acted as the first step of this interaction. Therefore, after seeding and culturing for 24 h on scaffolds in normal medium, BMSCs were immune-stained against β-integrin. As shown in Fig. 4A, a remarkably higher fluorescence signal was found in cells cultured on SF@MBG@Col scaffolds compared to those cultured on SF and SF@MBG. No significant difference was found between the SF and SF@MBG groups, which indicates the critical role of nanofibrous collagen. Results from western blotting (Fig. 4B) also confirmed that a higher level of β-integrin was detected in the hierarchical group ($p < 0.01$) as compared to the other two groups. Such an improvement was attributed not only to the nanofibrous structure, but also to the adhesive peptide within the backbone of collagenous fiber, such as RGD and GFOGER.[37] Since the involvement of the integrin pathway in osteogenesis activity has been reported,[38] the micro–nano hierarchical structure we put forward here could also take part in affecting the fate of progenitor cells.

As an anchor protein in focal adhesion that plays the role of a mechano-sensor during cellular adhesion and spreading,[39] vinculin was reported to be the regulator of stem cell differentiation mediated by the substrate properties, such as stiffness and the nano-scale structure. We assumed that the distinct actin fiber organization on hierarchical and non-hierarchical scaffolds was reflected by the distribution of vinculin in cells cultured on different structures. Hence, BMSCs cultured on scaffolds for 3 days in normal medium were immunostained against vinculin. As expected, a higher fluorescence signal was captured in cells cultured on the SF@MBG@Col scaffold (Fig. 4C), with the appearance of relatively brighter signals inside the cells. In comparison, green fluorescence was hardly seen in cells seeded on SF and SF@MBG, indicating the lack of focal adhesion formation and a poorly stretched cytoskeleton. Also, western blot along with its semi-quantification showed a significant difference in the expression of vinculin in BMSCs seeded on the hierarchical scaffold compared with the other groups ($p < 0.01$) (Fig. 4D).

YAP is another emerging mediator of cellular activity that is affected by mechanical and structural cues presented by the substrates.[33] In order to explore the potential effect of the hierarchical micro–nano structure on the YAP activity in co-cultured BMSCs, immunofluorescence was carried out to explore the localization of YAP in the cells seeded on different scaffolds. After co-culturing with the scaffold for 7 days in normal media, distinct localization of YAP within the cell was

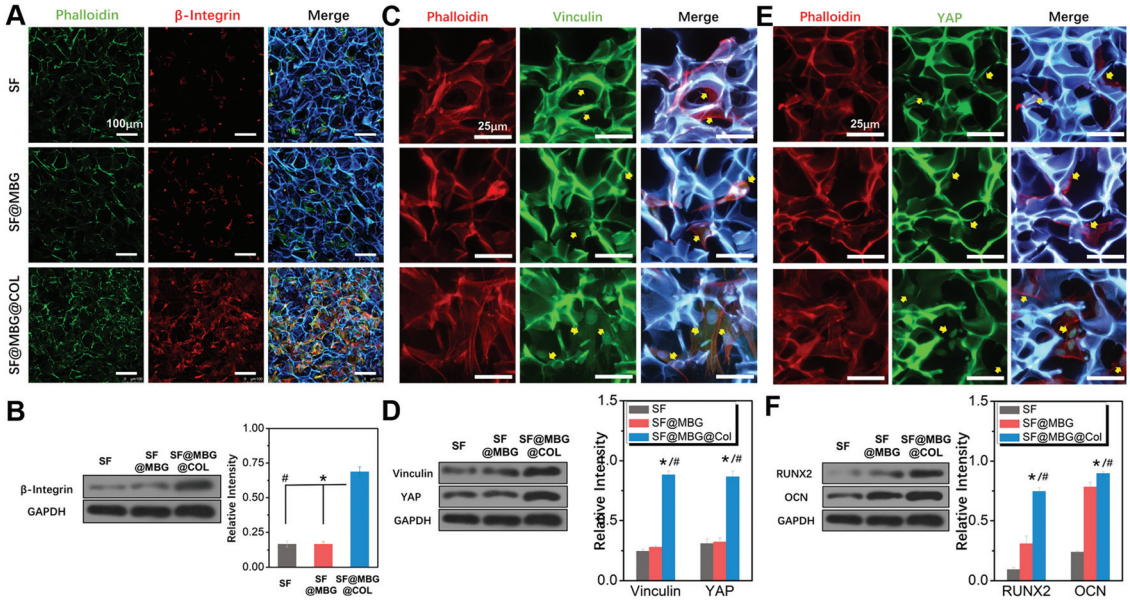

Fig. 4 Characterization of the mechanism behind structural cues. Immunofluorescence staining of (A) integrin in BMSCs co-cultured with the scaffold for 1 day and (C) vinculin and (E) YAP after co-culturing for 7 days, along with (B), and (D) their respective western blot followed by semi-quantification. (F) Western blot of RUNX2 and OCN in BMSCs after osteogenic induction followed by respective semi-quantification. (Statistical differences are indicated with $*p < 0.05$ when comparing SF@MBG@Col and SF@MBG, $\#p < 0.05$ when comparing SF@MBG@Col and SF, and $\&p < 0.05$ when comparing SF@MBG and SF.).

identified as shown in Fig. 4E, with the higher signal found in the nuclear sites of BMSCs seeded on the micro–nano scaffold. In comparison, a relatively lower signal was found in the nuclear site of the cells seeded on micro scaffolds, which was also reflected *via* the differences in western blot ($p < 0.01$) (Fig. 4D). Such a difference implied that the structure cue could participate in the activation of the YAP pathway within the cells to exert further effects.

The relevance of YAP/vinculin activity on the osteogenic effect of progenitor cells has been reported.[40,41] As osteogenic markers, Runt-related transcription factor 2 (RUNX2) and osteocalcin (OCN) were potentially affected by multiple pathways, such as integrin and stiffness-related vinculin/YAP pathways in the current scenario. Therefore, in order to access the general osteogenic effect of different scaffolds, western blot was performed to compare the expression level of RUNX2 and OCN in BMSCs seeded on different scaffolds for 7 days in osteogenic medium. Consistent with a previous study, as shown in Fig. 4F, significant higher levels of RUNX2 and OCN were identified in the SF@MBG@COL scaffold when compared with micro scaffolds ($p < 0.01$). A higher osteogenic marker expression has been found in the group with a micro–nano cue, indicating the final osteogenic effect of the hierarchical biomimetic structure.

Recently, studies on the biological effect of specific micro- or nano-structures on cells have come under the spotlight. A three-dimensional nanofibrous,[42,43] aligned fibrillar structure[44,45] and nano-scale topology[46,47] have been reported to exhibit significant impacts on the interaction between cells and materials from the point of adhesion, spreading, proliferation and further differentiation, potentially involving several pathways. In our work, the study of the mechanism behind the cytological effect of biomimetic hierarchical scaffolds remains on a comparatively shallow level. However, the current study provided the first hint on the potential mechanism of the osteogenic effect induced *via* the 3D micro–nano hierarchical scaffold and an overall advantage was noticed in our micro–nano structure which promotes the adhesion, spreading, proliferation and osteogenic differentiation of BMSCs through enhancing integrin, vinculin and YAP activities.

The *in vivo* performance of the scaffold was evaluated by using a rat cranial critical bone defect model. The scaffolds were applied to fill the space of the bone defect, as shown in Fig. 5A, and bone formation within the defect was characterized with the help of micro-computed tomography (μ-CT) at 8 and 12 weeks after the surgery. Histological analysis was conducted to observe the details of regeneration within the defect site at the points of 4 and 12 weeks post-surgery. Due to the osteoinductive effect of structural cues, a distinct regenerative pattern was expected between the hierarchical scaffold and non-hierarchical ones, as shown in Fig. 5B, which could indeed be verified by both micro-CT analysis and pathological evaluation.

As indicated in the 3D reconstruction image of the defect area (Fig. 5C), remarkable differences in bone coverage within the defect space were found; the SF@MBG@Col group exhibited significantly more new bone formation at both weeks 8 and 12. Also, the addition of MBG endowed the SF@MBG group with a superior capacity in promoting regeneration over the SF group. As verified by the 3D analysis of the defect area

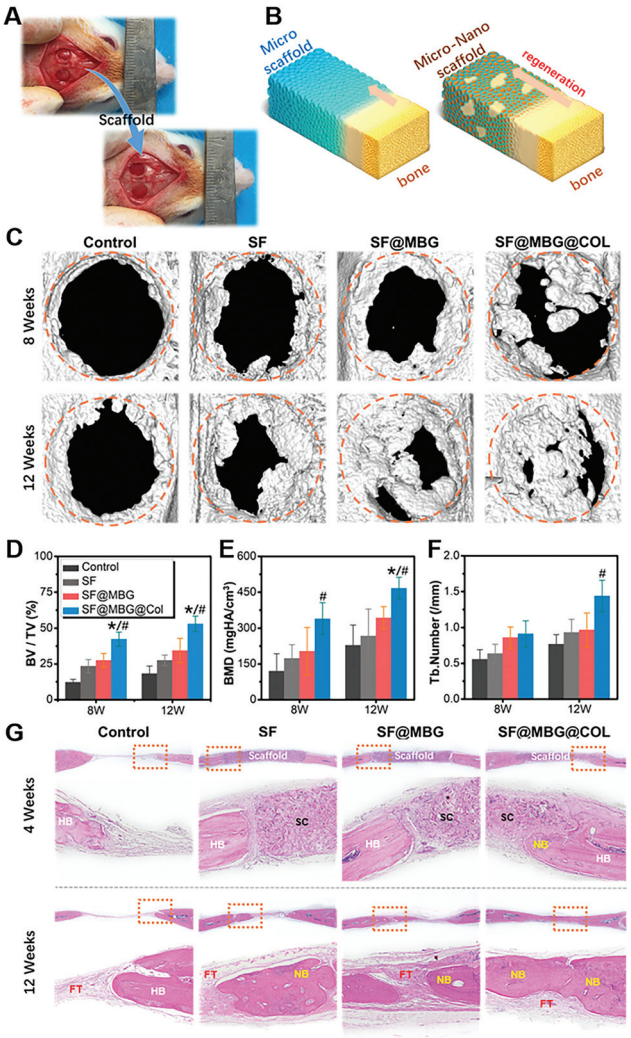

Fig. 5 Evaluation of the *in vivo* performance. (A) Photograph of a critical bone defect and implantation of scaffolds. (B) Illustration of the regenerative pattern of hierarchical and non-hierarchical scaffolds. (C) 3D reconstruction images of defect areas filled with different scaffolds. 3D analysis of (D) bone volume fraction (BV/TV), (E) bone mineral density (BMD) and (F) trabecular number (Tb. number) in the defect area. (Statistical differences are indicated with $*p < 0.05$ when comparing SF@MBG@Col and SF@MBG and $\#p < 0.05$ when comparing SF@MBG@Col and SF.) (G) H&E staining of the defect area at 4 and 12 weeks after surgery at a low and high magnification. The details are demonstrated with HB indicated as the host bone, NB as the newborn bone, LB as the lamellar bone, SC as the scaffold and FT as fibrous tissue.

(Fig. 5D–F), the corresponding tendency was found in these groups, with the hierarchical micro–nano groups showing a significantly higher bone volume to total volume ratio (BT/TV), bone mineral density (BMD) and trabecular number ($p < 0.05$). However, it is worth noting that a significant difference in the regeneration pattern between the hierarchical and non-hierarchical groups was identified. Such a difference arised because the SF@MBG@Col scaffold tended to promote the regeneration not only from the edge of the defect, but also from the inner area of the space that was in non-contact with the broken ends of the defect. We can infer that, apart from promoting the regeneration from the surrounding edge, the hierarchical micro–nano group was capable of inducing *in situ* regeneration within its biomimetic structure and completing the healing process with an inside-out style.

The regeneration of a bone defect is a complex process, in which, overgrowth of the regenerated bone, also known as ectopic bone formation, could potentially cause more problems.[48] The use of ectogenic bioactive factors or progenitor cells accounts for a substantial part of such unpleasant outcomes. The structural cues of the biomimetic scaffold could represent a potential alternative in this field due to their *in situ* regeneration and more controllable, natural-like regenerative process.

Histological analysis was further conducted to observe the topical details within the defect area. As shown by the HE staining images (Fig. 5G), at week 4, the scaffold remained intact in the implant site and the bone–scaffold interface was imaged to study the specific response. Compared with the clear boundary between the bone and scaffold in the groups of SF and SF@MBG, significant ingrowth of new bone was identified in the SF@MBG@Col scaffold, indicating its superior biocompatibility and capacity to induce early-stage osteogenesis. At 12 weeks after surgery, the scaffolds degraded completely. A similar trend was shown which is consistent with the micro-CT results. In the SF@MBG@Col group, uniform and continuous formation of new bone that covers the defect area was observed. In contrast, for the other groups, the defect areas were mainly filled with fibrous tissue (FT) and only partially regenerated bone, indicating inferior regenerative outcomes. Masson's trichrome staining also demonstrated a similar trend (Fig. S3A†). Since the mature collagen appeared red under Masson's trichrome staining, the significant advantage of SF@MBG@Col scaffolds was seen as indicated by the uniform regenerated bone with the newborn bone (NB) located at the center while mature lamellar bone (LB) covering the outer layer at 12 weeks. This phenomenon shared a higher similarity with the structure of normal calvarium. In comparison, the defect space implanted with SF and SF@MBG scaffolds was found to be filled with scattered newborn bone and FT. Moreover, deposition of collagen in regenerated tissue was visualized using immunohistochemistry (Fig. S3B†), which indicated both superior early stage osteointegration and later stage bone formation.

Conclusions

In this study, a biomimetic hierarchical scaffold inspired by natural bone formation was built through reinforcing the silk fibroin porous scaffold with nano-collagen and nano-bioglass from both inside the pore space and within the pore wall, relying on the ionic interaction between the carboxyl group from silk fibroin and the amine/calcium group from collagen/bioglass, bringing remarkably enhanced mechanical properties and structural integrity along with optimized biological

performance. A four times elevated compressive modulus was found on the SF@MBG@Col scaffold, as well as a dramatic impact on the adhering and spreading conditions of co-cultured cells reflected by the nearly three times expanded spreading area. Moreover, the structural cues presented by the hierarchical structure were found to affect the fate of progenitor cells and guide them to the osteogenic pathway. By evaluating the mechanism, the enhanced activity of osteogenic differentiation was found to be associated with the higher stiffness and hierarchically organized structure, which affected the fate of progenitor cells through the enhanced activities of integrin, vinculin and YAP. Furthermore, more uniform and rapid bone regeneration induced by structural cues over traditional non-hierarchical ones was identified. Overall, these results demonstrated a novel strategy for building biomimetic scaffolds through the application of integrated biomimetic compositions to achieve bone regeneration through structural cues.

Ethical statement

All animal procedures were performed in accordance with the Guidelines for Care and Use of Laboratory Animals of Soochow University and approved by the Animal Ethics Committee of the First Affiliated Hospital of Soochow University.

Conflicts of interest

There are no conflicts to declare.

Acknowledgements

Prof. L. C. acknowledges financial support from the National Natural Science Foundation of China (81772312, 81601891 and 81702190), Research and Development of Biomedical Materials and Substitution of Tissue and Organ Repair under the National Key R&D Program (2016YFC1101505), the Standardized Diagnosis and Treatment Project of Key Diseases in Jiangsu Province (BE2015641), the Natural Science Foundation of Jiangsu Province (BK20170370), the Natural Science Foundation of the Jiangsu Higher Education Institutions of China (15KJB320012), the Jiangsu Provincial Special Program of Medical Science (BL2012004), the Jiangsu Provincial Clinical Orthopedic Center, and the Priority Academic Program Development of Jiangsu Higher Education Institutions (PAPD). Prof. W. C. acknowledges financial support from the National Natural Science Foundation of China (51873107), the Shanghai Municipal Education Commission-Gaofeng Clinical Medicine Grant Support (20171906), the Shanghai Municipal Health and Family Planning Commission (201840027), Shanghai Jiao Tong University "Medical and Research" Program (ZH2018ZDA04), the Shanghai talent Development Fund (2018099). Prof. H. Z. acknowledges financial support from the Academy of Finland (grant no. 297580) and the Sigrid Jusélius Foundation (decision no. 28001830K1). Prof. H. A. S. acknowledges financial support from the HiLIFE Research Funds and the Sigrid Jusélius Foundation (decision no. 4704580).

Notes and references

1 T. N. Vo, F. K. Kasper and A. G. Mikos, *Adv. Drug Delivery Rev.*, 2012, **64**, 1292–1309.
2 K. W. Lo, B. D. Ulery, K. M. Ashe and C. T. Laurencin, *Adv. Drug Delivery Rev.*, 2012, **64**, 1277–1291.
3 J. M. Bouler, P. Pilet, O. Gauthier and E. Verron, *Acta Biomater.*, 2017, **53**, 1–12.
4 A. Malhotra and P. Habibovic, *Trends Biotechnol.*, 2016, **34**, 983–992.
5 J. Leijten, Y. C. Chai, I. Papantoniou, L. Geris, J. Schrooten and F. P. Luyten, *Adv. Drug Delivery Rev.*, 2015, **84**, 30–44.
6 D. X. Wei, J. W. Dao and G. Q. Chen, *Adv. Mater.*, 2018, **30**, e1802273.
7 X. F. Shen, Y. X. Zhang, Y. Gu, Y. Liu, B. Li and L. Chen, *Biomaterials*, 2016, **106**, 205–216.
8 K. S. Cahill, J. H. Chi, A. Day and E. B. Claus, *J. Am. Med. Assoc.*, 2009, **302**, 58–66.
9 B. Skovrlj, S. M. Koehler, P. A. Anderson, S. A. Qureshi, A. C. Hecht, J. C. Iatridis and S. K. Cho, *Spine*, 2015, **40**, 1862–1871.
10 C. Xu, P. Su, X. Chen, Y. Meng, W. Yu, A. P. Xiang and Y. Wang, *Biomaterials*, 2011, **32**, 1051–1058.
11 Y. Zhang, W. Fan, Z. Ma, C. Wu, W. Fang, G. Liu and Y. Xiao, *Acta Biomater.*, 2010, **6**, 3021–3028.
12 J. M. Holzwarth and P. X. Ma, *Biomaterials*, 2011, **32**, 9622–9629.
13 T. Xu, J. M. Miszuk, Y. Zhao, H. Sun and H. Fong, *Adv. Healthcare Mater.*, 2015, **4**, 2238–2246.
14 Y. Liu, D. Luo and T. Wang, *Small*, 2016, **12**, 4611–4632.
15 T. A. Einhorn and L. C. Gerstenfeld, *Nat. Rev. Rheumatol.*, 2015, **11**, 45–54.
16 S. C. Dennis, C. J. Berkland, L. F. Bonewald and M. S. Detamore, *Tissue Eng., Part B*, 2015, **21**, 247–266.
17 A. I. Alford and K. D. Hankenson, *Bone*, 2006, **38**, 749–757.
18 Y. R. Shih, C. N. Chen, S. W. Tsai, Y. J. Wang and O. K. Lee, *Stem Cells*, 2006, **24**, 2391–2397.
19 F. W. Kotch and R. T. Raines, *Proc. Natl. Acad. Sci. U. S. A.*, 2006, **103**, 3028–3033.
20 L. Chen, J. Hu, J. Ran, X. Shen and H. Tong, *Int. J. Biol. Macromol.*, 2014, **65**, 1–7.
21 G. Wu, H. Deng, T. Jiang, H. Tu, J. Chen, Y. Zhan, Y. Wang and X. Ma, *Colloids Surf., B*, 2017, **154**, 228–238.
22 J. Wang, F. Yu, L. Qu, X. Meng and G. Wen, *Biomed. Mater.*, 2010, **5**, 041002.
23 S. E. Bae, S. H. Bhang, B. S. Kim and K. Park, *Biomacromolecules*, 2012, **13**, 2811–2820.
24 L. Liu, J. Liu, M. Wang, S. Min, Y. Cai, L. Zhu and J. Yao, *J. Biomater. Sci., Polym. Ed.*, 2008, **19**, 325–338.
25 B. Narayanan, G. H. Gilmer, J. Tao, J. J. De Yoreo and C. V. Ciobanu, *Langmuir*, 2014, **30**, 1343–1350.

26 D. L. Christiansen, E. K. Huang and F. H. Silver, *Matrix Biol.*, 2000, **19**, 409–420.
27 Y. Pei, X. Liu, S. Liu, Q. Lu, J. Liu, D. L. Kaplan and H. Zhu, *Acta Biomater.*, 2015, **13**, 168–176.
28 A. J. Engler, S. Sen, H. L. Sweeney and D. E. Discher, *Cell*, 2006, **126**, 677–689.
29 E. Hoveizi, S. Ebrahimi-Barough, S. Tavakol and M. Nabiuni, *J. Biomed. Mater. Res., Part A*, 2015, **103**, 2952–2958.
30 M. C. Siebers, P. J. ter Brugge, X. F. Walboomers and J. A. Jansen, *Biomaterials*, 2005, **26**, 137–146.
31 A. J. Garcia, *Biomaterials*, 2005, **26**, 7525–7529.
32 T. Naganuma, *Nanoscale*, 2017, **9**, 13171–13186.
33 C. Yang, F. W. DelRio, H. Ma, A. R. Killaars, L. P. Basta, K. A. Kyburz and K. S. Anseth, *Proc. Natl. Acad. Sci. U. S. A.*, 2016, **113**, E4439–E4445.
34 J. Xie, D. Zhang, C. Zhou, Q. Yuan, L. Ye and X. Zhou, *Acta Biomater.*, 2018, **79**, 83–95.
35 C. K. Choi, Y. J. Xu, B. Wang, M. Zhu, L. Zhang and L. Bian, *Nano Lett.*, 2015, **15**, 6592–6600.
36 Y. Qian, H. Chen, Y. Xu, J. Yang, X. Zhou, F. Zhang and N. Gu, *Int. J. Nanomed.*, 2016, **11**, 4157–4171.
37 K. M. Hennessy, B. E. Pollot, W. C. Clem, M. C. Phipps, A. A. Sawyer, B. K. Culpepper and S. L. Bellis, *Biomaterials*, 2009, **30**, 1898–1909.
38 H. Liu, H. Peng, Y. Wu, C. Zhang, Y. Cai, G. Xu, Q. Li, X. Chen, J. Ji, Y. Zhang and H. W. OuYang, *Biomaterials*, 2013, **34**, 4404–4417.
39 X. Peng, E. S. Nelson, J. L. Maiers and K. A. DeMali, *Int. Rev. Cell Mol. Biol.*, 2011, **287**, 191–231.
40 H. Yuan, Y. Zhou, M. S. Lee, Y. Zhang and W. J. Li, *Acta Biomater.*, 2016, **42**, 247–257.
41 G. Abagnale, M. Steger, V. H. Nguyen, N. Hersch, A. Sechi, S. Joussen, B. Denecke, R. Merkel, B. Hoffmann, A. Dreser, U. Schnakenberg, A. Gillner and W. Wagner, *Biomaterials*, 2015, **61**, 316–326.
42 G. Kumar, C. K. Tison, K. Chatterjee, P. S. Pine, J. H. McDaniel, M. L. Salit, M. F. Young and C. G. Simon Jr., *Biomaterials*, 2011, **32**, 9188–9196.
43 T. Y. Cheng, M. H. Chen, W. H. Chang, M. Y. Huang and T. W. Wang, *Biomaterials*, 2013, **34**, 2005–2016.
44 Y. J. Ren, S. Zhang, R. Mi, Q. Liu, X. Zeng, M. Rao, A. Hoke and H. Q. Mao, *Acta Biomater.*, 2013, **9**, 7727–7736.
45 S. Wan, X. Fu, Y. Ji, M. Li, X. Shi and Y. Wang, *Biomaterials*, 2018, **171**, 107–117.
46 D. Carson, M. Hnilova, X. Yang, C. L. Nemeth, J. H. Tsui, A. S. Smith, A. Jiao, M. Regnier, C. E. Murry, C. Tamerler and D. H. Kim, *ACS Appl. Mater. Interfaces*, 2016, **8**, 21923–21932.
47 E. H. Ahn, Y. Kim, Kshitiz, S. S. An, J. Afzal, S. Lee, M. Kwak, K. Y. Suh, D. H. Kim and A. Levchenko, *Biomaterials*, 2014, **35**, 2401–2410.
48 R. Xu, J. Hu, X. Zhou and Y. Yang, *Bone*, 2018, **109**, 134–142.